Optimisation of Different Concrete Mix Designs for 3D Printing by Utilising 6DOF Industrial Robot

Pshtiwan Shakor[a], Jarred Renneberg[b], Shami Nejadi[a] and Gavin Paul[b]

[a]Centre for Built Infrastructure Research, School of Civil and Environmental Engineering, University of Technology Sydney (UTS), Australia
[b]Centre for Autonomous Systems, School of Electrical, Mechanical and Mechatronics, UTS
E-mail: {pshtiwan.shakor, Jarred.J.Renneberg}@student.uts.edu.au, {shami.nejadi, Gavin.Paul}@uts.edu.au

Abstract – Additive Manufacturing (AM) technologies are becoming increasingly viable for commercial and research implementation into various applications. AM refers to the process of forming structures layer upon layer and finds application in prototyping and manufacturing for building construction. It has recently begun to be considered as a viable and attractive alternative in certain circumstances in the construction industry. This paper focuses on the utilisation of different concrete mixtures paired with extrusion techniques facilitated by a six Degree of Freedom (DOF) industrial robot. Using methods of Damp Least Squares (DLS) in conjunction with Resolved Motion Rate Control (RMRC), it is possible to plan stable transitions between several waypoints representing the various print cross-sections. Calculated paths are projected via 'spline' interpolation into the manipulator controlled by custom software. This article demonstrates the properties of different concrete mixture designs, showing their performance when used as a filament in 3D Printing and representing a comparison of the results that were found. In this study, the prepared materials consist of ordinary Portland cement, fine sand between (425~150) micron, coarse aggregate ranges (3) mm and chemical admixtures which have been used to accelerate setting times and reduce water content. Numerous tests were performed to check the buildability, flowability, extrudability and moldability of the concrete mixtures. The horizontal test was used to determine the flowability and consistency, while the vertical and squeeze-flow tests were used to determine the buildability of the layers. The extrudability and moldability of the concrete mixtures were controlled by the robot and associated extruder speeds.

Keywords –
3D printing concrete**,** industrial robot, additive manufacturing, resolved motion rate control, squeeze-flow test, speed control, moldability.

1   Introduction

In most industrial segments, automation processes have significantly improved the efficiency of production. The construction industry, however, often seems to be slower to adopt automation in comparison to other industrial and manufacturing sectors. Therefore, significant efficiency improvements and economic benefits can be gained by the introduction of advanced automation into the construction process. With further automated development, manufacturing processes would take less time to complete, cost less and be more eco-friendly [5] & [8].

Lin et al.[15] state that the four main materials used in 3D Printing were composed of plastic, ceramic, metal and wax, and then in their research, they utilized rapid sulphoaluminate cement as the main binder.

It is obvious that AM plays a major role in the construction field. AM has powder base printing (D-shape) and Fused Deposition Modeling (FDM) method. FDM is well known as extrusion printing (printing via a robot) in the construction industry. In recent decades, a variety of technologies have been developed to implement additive manufacturing in the construction industry. These techniques can be divided into two print processes: Extrusion, and powder bed / inkjet 3D.

1.   Extrusion Printing

The extrusion printing technique involves extruding cementitious material from a nozzle attached to a framework to print structural layers, see Figure 1. For example, concrete printing, designed by Le [12] and contour crafting, established by Khoshnevis [10]. [13] investigated the hardened properties of high performance printed concrete that was extruded from a 9mm diameter nozzle. They demonstrated that the compressive strength of the printed samples in different directions is between 75 to 102 MPa. They also determined that the perpendicular load direction has the highest compressive load while in a conventional mould cast cube, has a compressive strength of approximately 107 MPa.
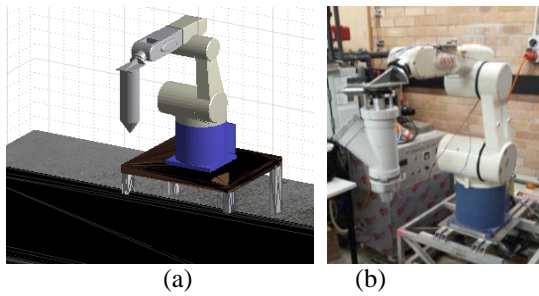
Figure 1. (a) Simulated Robot with a print nozzle assembly attached, for demonstrating and checking motion plans and paths. (b) Real world robot and auger nozzle assembly.

2.   Powder bed inkjet 3D printing

The powder printing fusion, i.e. powder-based 3DP, creates precise scaffolds with complicated geometries by dropping binder fluid (or "Toner") selectively into a powder bed to bind powder where it impacts the bed. [20] claimed that there is a post-hardening process which occurs after printing a specimen. It is possible to increase the compressive strength up to 35 MPa for Newberyite and up to 10 MPa for Struvite and the shrinkage level is 5-7% compared to the original model.

The main contribution of this paper is to show the materials extrusion method paired with the planning and control of the robot. The purpose is to demonstrate a series of different concrete mixtures and compare the results. There is potential for this process to create an automated method for manufacturing structural concrete columns and beams in both a pre-cast and cast in situ. This paper is organized as follows: Section 2 describes the materials and the methodologies used as well as the design and fabrication; Section 3   presents information regarding the analysis and testing methods used to find results; Section 4 discusses the results that were found from the experiments conducted. Section 5 provides a conclusion and proposes future work.

2   Materials and Methods

2.1   Materials

The materials in this study that have been used consist of ordinary Portland cement (General Purpose cement) by Eureka, fine sand (Sydney Sand) and coarse aggregate (10mm Blue Metal) both by Australian Native Landscapes and chemical admixtures such as superplasticizer (ADVA ® 650), water reducer (Daratard ® GP), accelerator (Sigunit L80AF), and retarder (Retarder N). Figure 2 shows the sieve analysis of fine sand and coarse aggregate. Moreover, the sieve analysis was done by the (Endecotts EFL2000) equipment. Later, the coarse aggregate has been crushed by the (Geo-Con) equipment to reduce the size of the

particles to about 3mm, see Figure 2 (b).
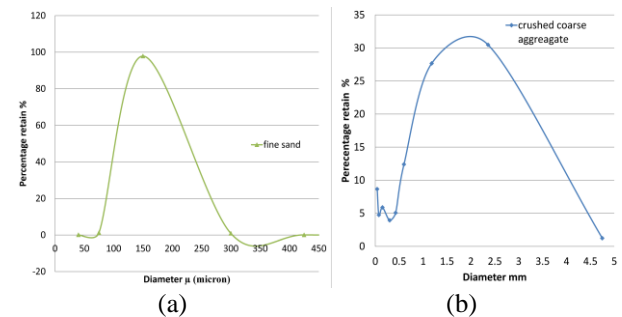
Figure 2. a) Sydney fine sand sieve analysis; b) Coarse aggregate sieve analysis after crushing.

2.2   Design and Fabrication

2.2.1 Extruder design

The extruder was made to adapt to the end-effector of the industrial robot (Denso VM6083), and was based on the design by [3]. The extruder consists of the following parts:

- Y-Pipe diameter (110)mm (Holman 100mm PVC 45 degree female and female plain junction)
- Truck wiper motor (24 Volts)
- Auger diameter(80)mm
- Nozzles with various sizes: circle (10, 20 and 30) mm, and square (10, 20 and 30) mm, (Figures 3).
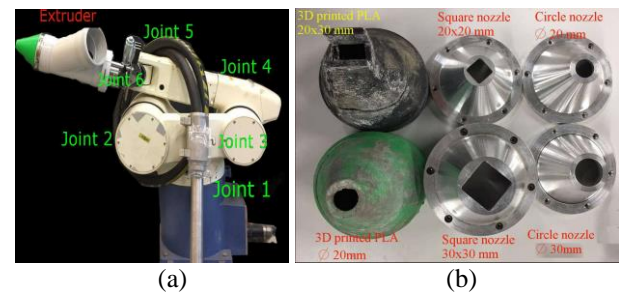
Figure 3. (a) Extruder joined to the Denso Robot. (b) Nozzle types made with Aluminium and PLA.

2.2.2 Materials mix design and fabrication

In this paper, several trials consisting of mixtures made of cement paste, cement mortar and concrete were performed. Fabrication and mix designs were prepared based on previous studies and literature.

[19] performed a meta-analysis regarding studies of concrete mix design, such as the study of [12], which was prepared as a cement-based mortar consisting of cement, silica fume, sand, fly ash and polypropylene fiber as the main ingredients. The optimum concrete mix design was found to be cement 579, sand 1241, fly

ash 165, silica fume 83 and water 232 (kg/m³). Furthermore, additional tests were conducted [14] to further optimize the mix with gypsum and cement while experimental tests of compressive strength found results in the range of 100-110 MPa.

[16] investigated the effects of superplasticizers on the flowability and buildability of cement mortar. In the mix with the high superplasticizer (0.95% to 2.5% of water weight), lower water-cement ratio content increases the compressive strength and flowability of the mix but it decreases the buildability capacity potentially. To build a 100mm high wall without any risk of failure, the optimum water-cement ratio and superplasticizer content (for better performance in flowability and buildability) was about 0.39 and 1.9% respectively, which used a nozzle diameter of 20 mm. In this study, an accelerator and retarder was added to control the rheology of the mortar.

Based on these mix design parameters we implemented a similar mix ratio in this paper.

2.3 Robot Planning and Control Methodology

To maintain a consistent flow it is important to implement an efficient method of planning to provide a stable path for the end-effector to follow. Using a combination of Damp Least Squares paired with Resolved Motion Rate Control to plan and control the robot's path, it is possible to create a steady 3-dimensional print which is completely customizable with an integrated MATLAB and C++ interface.

2.3.1 Damped Least Squares (DLS) Method

It is important to consider, when planning transitions between multiple joint states, how the robot will reduce the impacts of singularity on the system. A singularity refers to any given joint state of formation which reduces or even limits the degrees of freedom on the end effector. Typically, this occurs when two connected links form a straight member. The conventional method of calculating inverse differential kinematics results in a destabilization of the transitions between joint states. This appears, as described by Chiaverini et al. [6], as a sudden increase in joint velocities over large control deviations. It is possible to apply the DLS method (also known as Levenberg-Marquardt stabilization) in order to mitigate the impacts of singularities. This method reduces subsequent oscillations on the system as the joints approach an unreachable position. The DLS solution as appears in [4] can be described by the following equation,

$$\Delta\theta = (J^T J + \lambda^2 I)^{-1} J^T \vec{e}$$ (1)

Where the change in angular displacement, $\Delta\theta$, is minimised to stabilize the joint velocities when approaching a singularity. The damping constant, λ, must be adjusted [4] according to the systems' parameters in order to perform efficiently. Ahmed et al. [1] outlines how the stability of the rotational velocities depends heavily on the 'exactness' of the damping factor and that the damping constant can be found with the following equation:

$$\lambda = \lambda_0 \left(1 - \left(\frac{w}{w_0}\right)\right), \ w < w_0$$ (2)

where, λ_0, refers to the initial damping factor predetermined by [1] 'user requirements', and w refers to the measure of manipulability and w_0 refers to a threshold number of minimum manipulability before DLS is to be used.

For any given joint angle (θ_i, $i = 1, \ldots 6$) for all joint positions of the calculated path, a measure of manipulability of the system can be taken to determine whether or not the system is approaching a singularity. From Yoshikawa [21] we use the following equation,

$$w = \sqrt{\det(J * J^T)}$$ (3)

Where, J, is the Jacobian of the system, and J^T, is the transpose of the Jacobian, the measure of manipulability is compared to the predetermined threshold value represented by epsilon, ε (equal to w_0), which allows for the system to apply reactive coding to dampen the effects of singularity on the joint velocities for instance where the measure of manipulability, w, is less than ε.

The Jacobian of the system relates to the kinematic properties that are present during a transition at any given joint state. Acquiring the most appropriate joint velocity [2], for each individual joint involves using a Jacobian that relates both active and passive joint velocities acting in the system. As the robot is 6DOF, the system's Jacobian, J yields a 6×6 matrix. For any given path, the program will determine the required total joint positions by using inverse kinematics which yields the rotational joint positions q_i. The program stores these values in an n×6 matrix (where n is the number of joint positions required to transition through the given path), and then J is found by passing in q_i.

Depending on w at q, DLS will alter the way the Inverse Jacobian is calculated. When the manipulability is less than the threshold value represented by ε, a pseudo inverse Jacobian must be found in order to continue planning. This pseudo-inverse Jacobian is designed to handle stabilization issues associated with singularities, where the conventional method tends to perform poorly. The inverse Jacobian, J^+ is used to handle approach toward singularity as:

$$J^+ = J^T (J J^T + \lambda^2 I)^{-1}$$ (4).

2.3.2 Resolved Motion Rate Control (RMRC) Method

When considering a robot's joint motions there are multiple joint paths the robot can use in order to transition between consecutive end-effector poses [7]. For any given test represented by series of joint states, RMRC trajectory planning was used to create linear transitions between joint states. It allows the system to use the most optimal path between two points in space for where the robot's end-effector will transition with the best possible motion. Utilising the calculation of error for both the rotational and translational displacements, the program updates the stored joint rotational values, $\theta_{i=1 \rightarrow 6}$, in order to maintain a near linear trajectory. This also helps to maintain the end effectors' 'downwards' orientation during transitions.

Determining the joint velocities as shown in [11], drives the position of the end effector with a velocities,

$$\dot{x}_e = \left(\dot{x}_e, \dot{y}_e, \dot{z}_e, \dot{\theta}_r, \dot{\theta}_p, \dot{\theta}_y \right) \quad (5)$$

Since the end effector's Roll, θ_r, Pitch, θ_p, and Yaw, θ_y, are at fixed values, any change in velocity impacting on the end effector's change in position occurs linearly in the x, y, and z plane. The change in displacement is found using the following equation and stored as dx for each joint state, i, in any given transition:

$$dx = x_{i+1} - x_i, \ y_{i+1} - y_i, \ z_{i+1} - z_i \quad (6)$$

To maintain a fixed end effector roll, pitch and yaw, the rotational error of the end effector is calculated as,

$$d\theta = r_{i+1} - r_i, \ p_{i+1} - p_i, \ y_{i+1} - y_i \quad (7)$$

then used to correct the end effector's orientation as it transitions. The properties of both (6) and (7) are used to formulate the properties of (5), thus:

$$\dot{x}_e = (dx, d\theta) \quad (8)$$

Hewitt et al. [9] described the basis of RMRC as,

$$\dot{\theta} = J(\theta)^{-1} * \dot{x} \quad (9)$$

The calculated end effector velocity, $\dot{x}$, is found in (8). Depending on whether DLS is implemented the inverse Jacobian, denoted by $J(\theta)^{-1}$, with the end effector velocity will give the required rotational velocities, $\dot{\theta}$, for each joint.

The robot uses the angular velocity, $\dot{\theta}$, to apply RMRC to update the next joint state parameters based on the current joint positions. This method applies an element of self-correction to the path planning to ensure that the end-effector maintains the same direction.

2.3.3 End-Effector Velocity

Finding the actual velocity of the end-effector is essential for maintaining an effective extrusion rate at the end-effector. Note that despite the use of RMRC in the planning of the robot's path, the actual joint step completion time is determined by the controller. Given the maximum joint velocities of each joint, it is possible to calculate the maximum 'actual' velocity of the end effector at any given time. Equation (9) can be re-arranged to give the following:

$$\dot{x} = J(\theta) \cdot \dot{\theta} \quad (10)$$

Essentially, calculating the product between the Jacobian for a given joint state and the rotational velocities will give the velocity components of the end effector. By accounting for the percentage multipliers imposed by the controller pipeline, (10) is expressed as:

$$\dot{x} = P_M * P_{TP} * (J(\theta) \cdot \omega) \quad (11)$$

Where P_M and P_{TP} are the percentage values of maximum speed dictated by the software interface and the robot's teach-pendant, respectively. Finding the magnitude of $\dot{x}$ gives the controlled peak velocity. For the experiments these values were heuristically determined by measuring both the displacement of a given path and time to complete the path.

3 Analysis and Testing

3.1 Squeeze-flow Test

Several tests have been conducted to evaluate the mechanical properties of the materials prior to printing complete structures. The tests are arranged based on the cement mortar and concrete materials properties. All the trails are listed in Tables 1 and 2.

The squeeze-flow test is prepared according to Brazilian test (ABNT NBR 15839). The machine used to prepare the test is the Shimadzu, (50kN, Japan). The displacement speed is approximately 0.1 mm/second (Figure 4, ONP). The surface roughness test is conducted by a portable profile-meter (Taylor Hobson Surtronic 3+). Tests are performed for the single, double and triple layers, in order to evaluate the buildability of layers.
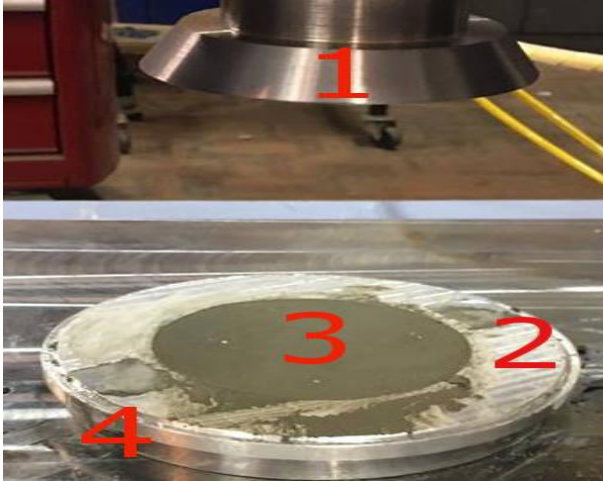
Figure 4. The squeeze flow configuration: (1) top plate diameter (101 mm), surface roughness (Ra0.0586); (2) mould ring diameter (101 mm) and height (10 mm); (3) cement mortar sample; and (4) bottom plate diameter (160 mm), surface roughness (Ra 0.0586).

3.2 Robot Planning and Control Tests

3.2.1 Horizontal and Vertical Tests

The main transition path that the robot takes, referred to as the 'horizontal test', is shown in Figure 5 and consists of a series of rows of approximately 300mm in length printed next to each other. The distance between the layers (in the y direction) is determined by the desired thickness of the layer which is reflected by the choice in nozzle. The 'vertical' test was simply the same footprint except after completing the tenth line the end-effector would return to the starting position, increment upwards and repeat the same pattern.
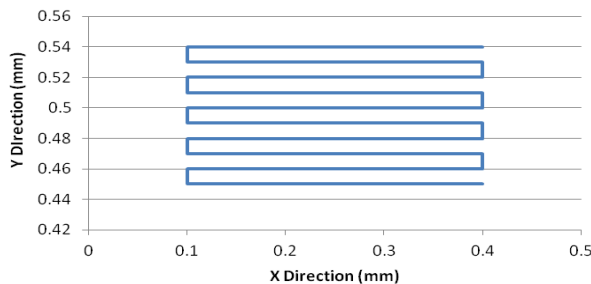
Figure 5. 'Horizontal Test' cross-section path.

3.2.2 Oscillation Damping with DLS

The different velocity components that act in the system have significant impacts on the shape of the extruded mortar and concrete mixtures. The auger delivery method impacts directly on the flow rate of the mixture flowing from the extruder. Secondarily,

reducing the effects of joint oscillations as the robot approaches singularities is essential to maintain a smooth print result. Tests are conducted to show the impact of the DLS method on joint velocities as a joint's measure of manipulability reduces.

Table 1: Trials prepared by an extruder for cement mortar

Trial No.	C (g)	FS (g)	W (ml)	R (ml)	Acc (ml)	SP (ml)	WR (ml)	Noz (mm)
1	1000	0	360	8	4	10.4	-	∅20
2	1000	500	300	8	4	10.4	-	∅20
3	500	500	150	4	4	5.2	-	∅20
4	750	750	292.5	4	4	5.5	-	∅20
5	750	750	250	4	5	5	-	∅20
6	1500	1500	550	8	10	11	-	20×20
7	1000	1000	361.6	5.33	6.6	6.67	-	20×20
8	1000	1000	343	5.33	6.6	6.67	-	20×20
9	1000	1000	350	5.33	6.6	6.5	-	20×20
10	1000	1250	375	5	6	5	3	∅10

C:cement, FS:fine sand, W:water, R:retarder, Acc:accelerator, SP:superplasticizer, WR:water reducer, Noz:nozzles

Table 2: Trials for crushed coarse aggregate by an extruder

| Trial No.	C (g)	FS (g)	A (g)	W (ml)	R (ml)	Acc (ml)	SP (ml)	WR (ml)	Noz. (mm)
11	750	750	250	300	4	5	5	-	20×20
12	750	750	250	250	4	5	5	-	20×20

4 Result and Discussion

Experimental trials were conducted to determine the effectiveness of the mortar or concrete mixtures. Based on the consistency and rheology of the printed samples, several trials were chosen as 'optimum' trials for the squeeze flow tests and compressive strength tests. The ring moulds were prepared for squeeze flow test.

Several mix designs performed similarly to the mixtures presented in previous studies by [12], [14], [16], [19]. Furthermore, these tests also depend on the capabilities of the extruder, see Table 3.

There were 12 different concrete mix design trials which were performed by the 6DOF industrial robot. Out of these trials, only three were chosen for their performance in compressive strength and results yielded in the squeeze-flow test. These tests were the basis for the printing quality test, flow quality and the buildability (i.e. each layer's capability of holding subsequent layers without falling). These benchmarking keys for printing have been stated by [17], [13], [19]. Generally, the thickness for the printed line changed in a range of about (1-2) mm. According to Table 3, the thickness for each printed line for the different nozzle provided different results.

In addition, it was determined that the quality resolution of materials also depended on the speed of
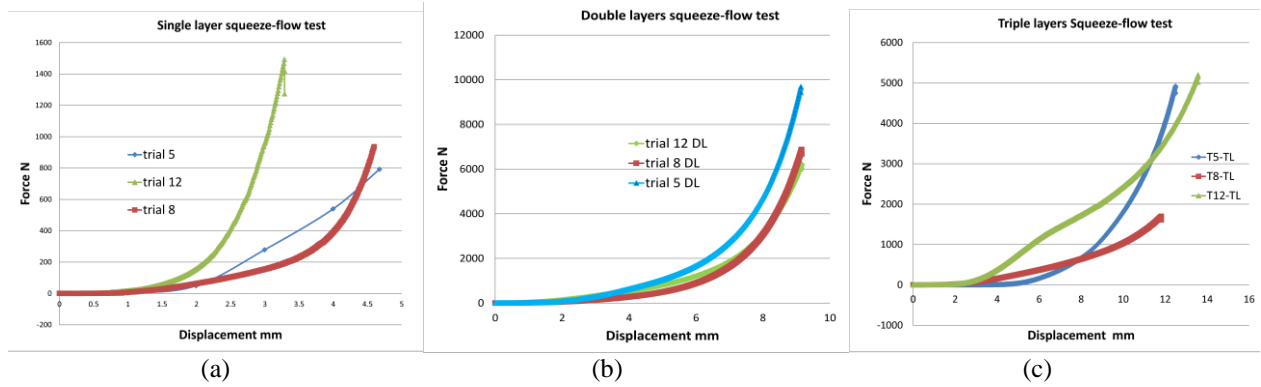
Figure 6. Squeeze-flow graph for the single layer, double layers and triple layers of different concrete mix

auger (flow rate) and velocity components associated with the various joints of the robot.
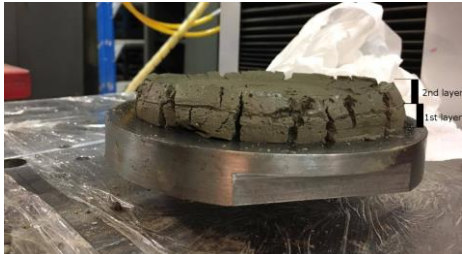
4.1 Squeeze-flow test

The squeeze flow tests showed different results for single, double and triple layers of the selected mixtures, as shown in Figure 6. In a test that uses a single layer the concrete mixture had higher results in force until it reached the required displacement. For example, at the displacement 2.99mm, the required load in Trial 12 (concrete mix with small aggregate) was about 956.51 N. At the same displacement for Trials 5 and 8 (cement mortar) the load was about 277.82 N and 153.11 N, respectively. When examining the results of tests that utilized a double layer there were significant differences in comparison to the single layer results. Trial 5 (cement mortar) had a force which reached approximately 622.54 N when at a displacement of about 3.99 mm, while for Trials 12 and 8 the loads were 536.05 N and 275.75 N, respectively. At the same displacement, the results for the triple layers exhibit a similar pattern.

These results show that the mortar is more coherent than the concrete mixtures. Thus, it does not allow air entertained bubbles to remain in the mortar mixture. In the study by [18], it was discovered that the mortar in the first 24 hours of early age had a greater compressive strength in comparison to normal concrete. Hence, a much higher percentage of open pores will exist in the concrete mixtures in comparison to cement mortar due to the presence of aggregates. The larger particle sizes encourage porosity within the concrete mixtures.

The force is dependent on the number of chains and the force between the particles. In the Trial 12 single layer test the mixture contained small particles of coarse aggregate. It can be determined that because of the presence of small aggregate particles the mixture was capable of resisting more force over the given displacement, Figure 6. Moreover, it shows that the mortar mix could handle more layers than the concrete mix and less penetration will occur between layers in mortar mix when loads are applied (Figures 6 and 7).

Table 3: Several printed specimens shapes with comments

Trial Number	Image	Comment
Trial 5		Successful print
Trial 7		Slightly flow
Trial 8		Good layers

Figure 7. Squeeze-flow for the double layers of trial 12

4.2 Extruder Delivery and Speed Control Results

It was crucial that the mortar or concrete mix designs were compatible with the speed of robot and the auger delivery methods. Researchers like Hwang and Khoshnevis [10] had mechanical speed limitations with the novel contour crafting system; the speed of the
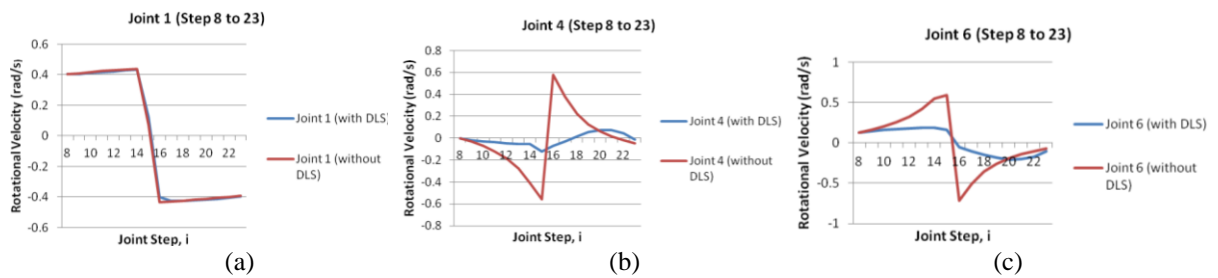
Figure 9. Velocity comparison for joints: (a) 1, (b) 4, and (c) 6.

material deposition was not well established in their research. It was also identified that robot in use was limited to a reach of approximately 1100mm from the base. Printed specimen dimensions are thus limited to be contained within this workspace.

Mixtures that had reduced workability were severely impacted when the velocity of the end effector was excessively fast. The robot ran the calculated path at a constant velocity before the extruder had time to move a proper volume of material. This resulted in layers with significant gaps between them. Alternatively, mixtures with increased workability were negatively impacted when the velocity of the end-effector was too slow. These instances would result in the robot moving too much volume of material before the robot could properly transition through the calculated path.

Regarding the auger delivery method, it was important to determine an appropriate velocity in which the end-effector would travel paired with a suitable supply voltage to the 24V motor which powered the extruder's auger to form an acceptable flow. It was found that the auger could move substantial volumes of material. However, the flow rate tended to be inconsistent. Material tended to gather on the inside of the extruder tubing and allowed the formation of air pockets in the flow. Despite this, it was determined that the optimal speed for the robot was between 39.36 and 42.12 mm/sec when the auger voltage was set to approximately 15 to 19 volts. Another drawback was that the motor that powered the auger struggled to rotate when put under increased loads. Loads from the mixes with higher densities and higher viscosities reduced the augers' practicality considerably.

As the robot's layer height increased the more contorted the required joint angles were. The manipulability was significantly reduced at some points of the path and DLS was required to dampen the resulting oscillations. The immediate goal for the vertical print test was to get to an ultimate print height of approximately 600mm (Figure 5 shows the cross section). For the following graphs, the robot was set to print the vertical test at a height of 590mm from the printing plate with a layer thickness of 10mm. The process was discretized into approximately 130 robot
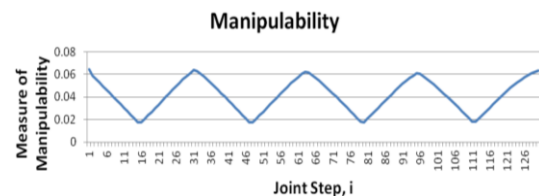
Figure 8. Measure of Manipulability

poses in order to complete each layer.

Figure 8 shows that the system utilized DLS on several occasions. The robot approaches singularity between joint step intervals of 8 – 23, 40 – 56, 72 – 88 and 103 – 120 (manipulability is less than 0.4), and the system implements DLS during these intervals to reduce the sudden change in rotational velocity.

Figures 9 depict the change in rotational velocity for joint states from joint step 8 to joint step 23. Take note that the other joint step intervals yield similar results; hence, only one interval is examined.

It can be seen that the smallest changes occur in Joint 1. Joint 4 and Joint 6 show significant damping. This could be due to the fact that these joints have a much larger displacement requirement in comparison to the other joints. The most significant change in rotational velocity occurs between steps 16 and 17. With DLS the change in velocity is significantly smoother in comparison to without DLS.

5 Conclusions

This paper has presented the initial stages involved in developing a working model of 3D printed concrete lines by using a 6DOF Industrial Robot. It has detailed the mix design properties used and how these mixes have been evaluated by several trials and tests. It has found that the impact of the optimum material mixes and the use of DLS paired with RMRC to control joint velocities are crucial in establishing good printing foundations. The results showed that mortar is more capable in printing and building layers due to less voids and porosities between particles, while the concrete mixes form openings and significantly more internal spacing for the air entertaining. It is evident that these studies need to be further developed and tested with different ages of curing samples, testing for compressive strength and checked with the controlled samples.

For future works, it is intended that improvements and additions to the system will continue to be developed. Performing compressive strength tests will be a focus for short term goals. Due to the inconsistency of flow rates provided by the auger, there will be considerable effort to move to a pump delivery system. Furthermore, an investigation to optimise the parameters of the model will occur so as to increase the accuracy of planning and control of the robot. Additionally, the plan is to work on predictive models, online sensing and feedback to reduce the chance of errors and thus improve both system safety and robustness.

6   Acknowledgements

7   REFERENCES

[1]   S.M. Ahmed, A.N. Pechev, Performance analysis of FIK and DLS inverse kinematics using six degree of freedom manipulator, Robotics and Biomimetics, 2009 International Conference IEEE, 2009, pp. 1405-1410.

[2]   O. Altuzarra, O. Salgado, V. Petuya, A. Hernández, Computational kinematics for robotic manipulators: Jacobian problems, Engineering Computations 25 (1) (2008) 4-27.

[3]   L. Anell, Concrete 3d printer, Master Thesis, Department of Design Science, Lund University, 2015.

[4]   S.R. Buss, Introduction to inverse kinematics with jacobian transpose, pseudoinverse and damped least squares methods, IEEE Journal of Robotics and Automation 17 (1-19) (2004) 16.

[5]   R.A. Buswell, R. Soar, A.G. Gibb, T. Thorpe, The potential of freeform construction processes, (2005).

[6]   S. Chiaverini, B. Siciliano, O. Egeland, Review of the damped least-squares inverse kinematics with experiments on an industrial robot manipulator, IEEE Transactions on Control Systems Technology (2) (1994) 123-134.

[7]   M. Clifton, G. Paul, N. Kwok, D. Liu, D.-L. Wang, Evaluating performance of multiple RRTs, Mechtronic&Embedded Systems and Applications, 2008. MESA 2008. International Conference IEEE, 2008, pp. 564-569.

[8]   L. Edwards, C. Holt, L. Keyte, R. Lloyd, Construction 3D Printing, (2015).

[9]   J. Hewit, J. Love, Resolved motion rate control of a materials-handling machine, Transactions of the Institute of Measurement and Control 5 (3) (1983) 155-159.

[10]   D. Hwang, B. Khoshnevis, Concrete wall fabrication by contour crafting, 21st International Symposium on Automation and Robotics in Construction (ISARC 2004), Jeju, South Korea, 2004.

[11]   N.Y. Ko, Extended RMRC and its Application to the Motion of a Mobile Manipulator, International Journal of Humanoid Robotics 12 (02) (2015) 1550016.

[12]   T.T. Le, S.A. Austin, S. Lim, R.A. Buswell, A.G.F. Gibb, T. Thorpe, Mix design and fresh properties for high-performance printing concrete, Materials and Structures 45 (8) (2012) 1221-1232.

[13]   T.T. Le, S.A. Austin, S. Lim, R.A. Buswell, R. Law, A.G.F. Gibb, T. Thorpe, Hardened properties of high-performance printing concrete, Cement and Concrete Research 42 (3) (2012) 558-566.

[14]   S. Lim, R.A. Buswell, T.T. Le, R. Wackrow, S.A. Austin, A.G.F. Gibb, T. Thorpe, Development of a viable concrete printing process, (2011).

[15]   X. Lin, T. Zhang, L. Huo, G. Li, N. Zhang, J. Liao, Preparation and Application of 3D Printing Materials in Construction, (2015).

[16]   Z. Malaeb, H. Hachem, A. Tourbah, T. Maalouf, N. El Zarwi, F. Hamzeh, 3d Concrete Printing: Machine And Mix Design, International Journal of Civil Engineering (6) (2015).

[17]   B. Panda, Y. Tay, S.C. Paul, T.M. Jen, K. Leong, I. Gibson, Current Challenges And Future Perspectives Of 3d Concrete Printing.

[18]   P.S. Surendra, A. Yilmaz, V. Thomas, Determination of Early Age Mortar and Concrete Strength by Ultrasonic Wave Reflections, (2003).

[19]   Y.W. Tay, B. Panda, S.C. Paul, M.J. Tan, S. Qian, K.F. Leong, C.K. Chua, Processing and Properties of Construction Materials for 3D Printing, Materials Science Forum, Vol. 861, 2016.

[20]   E. Vorndran, K. Wunder, C. Moseke, I. Biermann, F.A. Müller, K. Zorn, U. Gbureck, Hydraulic setting $Mg_3(PO_4)_2$ powders for 3D printing technology, Advances in Applied Ceramics 110 (8) (2011) 476-481.

[21]   T. Yoshikawa, Manipulability of robotic mechanisms, The international journal of Robotics Research 4 (2) (1985) 3-9.